Solar Energy Materials & Solar Cells 154 (2016) 99–103

Contents lists available at ScienceDirect

Solar Energy Materials & Solar Cells

journal homepage: www.elsevier.com/locate/solmat

Improved empirical method for calculating short circuit current density images of silicon solar cells from saturation current density images and vice versa

O. Breitenstein [a,*], F. Frühauf [a], M. Turek [b]

[a] Max Planck Institute of Microstructure Physics, Halle, Germany
[b] Fraunhofer Center of Silicon Photovoltaics (CSP), Halle, Germany

ARTICLE INFO

Article history:
Received 23 December 2015
Received in revised form
26 April 2016
Accepted 27 April 2016
Available online 10 May 2016

Keywords:
Quantitative evaluation
Photocurrent imaging
Lock-in thermography
Photoluminescence imaging
Local analysis

ABSTRACT

An empirical dependence of the short circuit current density J_{sc} as a function of the dark saturation current density J_{01} is proposed, which describes this dependence down to a bulk lifetime of 1 ns. This method avoids artifacts, which appear when applying the previously proposed quadratic dependence. The parameters of the new dependence are fitted to PC1D simulations and to experimental LBIC results for various wavelengths and AM 1.5 for a typical industrial BSF-type solar cell and a PERC cell. This dependence can also be used to calculate J_{01} images from LBIC-based J_{sc} images. It turns out that this method is more reliable in BSF than in PERC cells.

1. Introduction

The local short circuit current density $J_{sc}(x,y)$ of a solar cell, which is an important local efficiency parameter in particular for multicrystalline silicon solar cells, is usually imaged by LBIC mapping at a certain wavelength, see e.g. [1]. If the mapping is performed with different wavelengths, an image of J_{sc} under AM 1.5 illumination may be obtained, see [2]. Recently, both illuminated lock-in thermography (ILIT) [3] and dark lock-in thermography (DLIT) [4] based methods for imaging J_{sc} were proposed. The basic idea of the DLIT based method is that the local dark saturation current density J_{01} is a measure of the local bulk recombination probability. Therefore this parameter should also govern bulk recombination under short-circuit condition, which governs the local value of J_{sc}. An advantage of this method is that it can be applied to J_{01} images obtained by any imaging method, even to images that have been captured in the past. In particular this method is a good extension of the "Local I-V 2″ method for evaluating DLIT images, which is currently the most reliable method to image J_{01} and perform a local efficiency analysis of given inhomogeneous solar cells, see [5–7].

In the previous empirical method for imaging J_{sc} [4] it was found that and explained why the reduction of J_{sc} with increasing J_{01} is linear in J_{01} only for small values of J_{01} and gradually saturates for higher values, corresponding to lower bulk lifetimes. In this work [4] the fit of PC1D-based (see [8]) J_{01}-dependent J_{sc} values was performed up to a maximum of $J_{01}=5^{*}10^{-12}$ A/cm^2. In this range, the dependence $J_{sc}(J_{01})$ could be well approximated by a quadratic function, hence by a 2nd order polynomial. However, when this method was later applied in practice and J_{01} values above $5^{*}10^{-12}$ A/cm^2 appeared, this lead again to an apparent increase of J_{sc} with increasing J_{01}, which is clearly physically wrong. Therefore the goal of this contribution is to find a physically more reliable description of the $J_{sc}(J_{01})$ dependence, which does not show this non-monotonic behavior and can be used up to very high values of J_{01}. This new dependence will first be fitted to PC1D simulations of a standard industrial BSF-type and a PERC-type multicrystalline silicon solar cell. Then, on typical cells of both types, LBIC images taken at AM 1.5 and various discrete wavelengths are compared with DLIT-based J_{01} images, leading to more realistic sets of fitting parameters.

2. The method

First we simulate J_{sc} and J_{01} by PC1D [8] for a typical industrial BSF-type cell of first generation with full-area Al back contact and for a PERC cell, in both cases for widely varying values of the bulk lifetime τ_{bulk}. The used simulation parameters are the same as in [4], namely 200 μm cell thickness, $p_0=1.5^{*}10^{16}$ cm^{-3}, and $T=25$ °C

* Corresponding author.
E-mail address: breiten@mpi-halle.mpg.de (O. Breitenstein).

http://dx.doi.org/10.1016/j.solmat.2016.04.047
0927-0248/

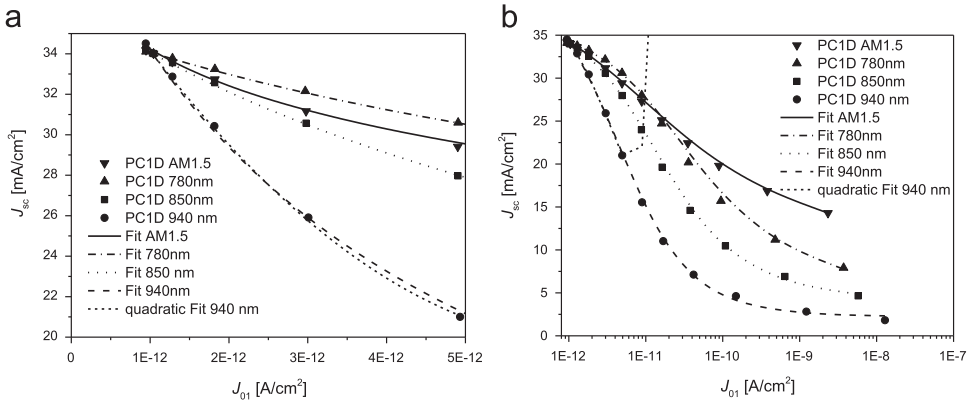

Fig. 1. Dependence of J_{sc} on J_{01} for a standard cell, (a) linear drawing up to $J_{01}=5*10^{-12}$ A/cm^2, (b) linear over log(J_{01}) in the whole range. Symbols: PC1D simulations, lines: Fits.

for both cells, $J_{01}^e=550$ fA/cm^2 and $S_{rear}=600$ cm/s for the standard cell, and $J_{01}^e=90$ fA/cm^2 and $S_{rear}=10$ cm/s for the PERC cell. Whereas in [4] the simulations have been performed for τ_{bulk} from 1 ms down to 1 μs, corresponding to J_{01} up to $5*10^{-12}$ A/cm^2, the simulations are performed here for τ_{bulk} from 10 ms down to 1 ns, corresponding to J_{01} up to 10^{-8} A/cm^2. As in [4] the values of J_{01}^e and S_{rear} are assumed to be independent of τ_{bulk}, which is only an approximation. All PC1D simulations were made for monochromatic illumination at 780, 850, and 940 nm and for AM 1.5 G (1 sun). The intensity for the monochromatic illumination was chosen so that, at a bulk lifetime of 100 μs, the monochromatic J_{sc} is equal to that at AM 1.5. In the PC1D simulations we calculate J_{01} from simulated values of J_{sc} and V_{oc} by applying a simple one-diode model with an ideality factor of unity. This is certainly not correct for very low lifetimes, where recombination in the depletion region becomes important, but is accurate in the region up to $J_{01}=1.5*10^{-11}$ A/cm^2, where the experimental LBIC data will be fitted.

Fig. 1 shows PC1D simulations of $J_{sc}(J_{01})$ for the standard BSF-type cell as symbols (a) with a linear scale up to $J_{01}=5*10^{-12}$ A/cm^2 and (b) over the logarithm of J_{01} in the full simulation range. The results for the PERC cell look qualitatively similar, except that here the J_{01} values already start in the low 10^{-13} A/cm^2 range. In Fig. 1(a) and (b) the result of a quadratic fit of $J_{rec,sc}(J_{01})$ for the 940 nm data in the range below $J_{01}=5*10^{-12}$ A/cm^2 is also shown. We see in (a) that this fit is quite good in this fitting range, but (b) shows that for higher J_{01} the values of J_{sc} drastically increase again. The goal of this paper is to find a better empirical description of $J_{sc}(J_{01})$, which holds over the whole definition range of J_{01} and shows a monotonic dependence on J_{01}.

The short circuit current represents the quantum efficiency of a solar cell, where the diffusion length L_d of the minority carriers, depending on the bulk lifetime τ, enters as a crucial parameter. Similarly, the dark saturation current density is directly related to the diffusion length. Let us first look for the two limiting cases of the bulk thickness being much larger and much smaller than L_d and L_α, respectively. These two limiting cases should also be met by our empirical formula for $J_{sc}(J_{01})$. In a first simplified approach for bulk thickness larger than L_d and L_α we find $J_{sc}\sim IQE=1/(1+L_\alpha/L_d)$ (see [9]) and $J_{01}=(eDn_i^2)/(N_AL_d)$ (see [10]), leading to:

$$J_{sc}(J_{01}) \sim \frac{1}{1+\frac{J_{01}L_\alpha N_A}{eDn_i^2}} \tag{1}$$

Here L_α is the absorption length, D the diffusion constant, n_i is the intrinsic carrier concentration, and N_A the bulk doping concentration. This dependence is constant for low values of J_{01} and approaches zero for large J_{01}. However, it has to be considered that (1) only covers the bulk contribution of J_{sc}. There is also an emitter and depletion region contribution of J_{sc}, which does not depend on the bulk lifetime. Hence in reality even for very large J_{01} (low bulk lifetime), J_{sc} is expected to drop to a finite value, which should depend on the excitation wavelength governing L_α. In the second limiting case, where bulk thickness d smaller than L_d and L_α we find $J_{sc}\sim 1-c1/\tau$ (here $c1$ is a constant) and $J_{01}=(en_i^2d)/(N_A\tau)$ (see [11]), leading to:

$$J_{sc}(J_{01}) \sim 1-c2J_{01} \tag{2}$$

Here $c2$ is another constant. This dependence drops linearly for low values of J_{01}, where it should be valid. The derivation of a strict analytical relationship between J_{sc} and J_{01}, which is applicable to real solar cells and includes the spectrum of the light, the inhomogeneity of the cell, its optical properties and contributions from emitter and space charge regions, would be very complex. Thus, our proposal is a phenomenological expression, which contains only four free parameters A, B, C, and n, but nevertheless yields a very good representation of the numerical and experimental data. We have found that the $J_{sc}(J_{01})$ dependence can be well fitted by:

$$J_{sc}(J_{01}) = C-\frac{AJ_{01}}{\left[1+\left(\frac{AJ_{01}}{B}\right)^n\right]^{\frac{1}{n}}} \tag{3}$$

For low values of J_{01} this dependence drops linearly with J_{01} as in (2), whilst for very large values it approaches a finite value as in (1), regarding its discussion. The parameter A (dimensionless) in (3) describes, as in [4], the slope of the dependence in the linear part for low J_{01} values. This parameter describes the limiting case of small J_{01} after Eq. (2), where it corresponds to the parameter $c2$. The parameter B (in units of A/cm^2) describes the saturation value of the reduction (drop) of J_{sc} for large J_{01}. According to Eqs. (1) and (3), $B\sim eDn_i^2/(L_\alpha N_A)$ holds, assuming $n=1$ (the factor A in the nominator and the denominator cancel for large J_{01}). The parameter n (dimensionless) describes how fast the dependence saturates (large n means fast saturation and small n means slow saturation), and the offset parameter C (in units of A/cm^2) describes the J_{sc} value for an assumed J_{01} of zero. These parameters hold globally for certain types of cells (e.g. standard or PERC) and certain illumination conditions. Note that, for varying light intensity or reflection properties, the parameters A, B, and C scale linearly with the light intensity, but parameter n does not. This becomes clear by considering the limiting cases for low and high J_{01}, leading after (3) to $J_{sc}^{low}=C$ and $J_{sc}^{high}=C-B$, which both must be proportional to the illumination intensity, and also the slope factor A should be proportional to the drop amount B. As a good approximation it can be assumed that these parameters scale with the global mean value of the short circuit current density of the cell. The lines in Fig. 1 show the fitting results for all illumination

conditions and Table 1 shows the obtained fitting parameters, also for the PERC case. We see that now the fit is possible over 4 orders of J_{01} up to 10^{-8} A/cm^2.

As in [4] the offset parameter C may now be expressed by the global mean value of $<J_{sc}>$ of the cell, if this is known. For the mean value of the short circuit density we obtain from (3):

$$<J_{sc}> = C - \sum_i \frac{AJ_{01,i}}{N\left[1+\left(\frac{AJ_{01,i}}{B}\right)^n\right]^{\frac{1}{n}}} \quad (4)$$

where (N= number of pixels). This leads, using (3), to the final result:

$$J_{sc,i} = <J_{sc}> - \frac{AJ_{01,i}}{\left[1+\left(\frac{AJ_{01,i}}{B}\right)^n\right]^{\frac{1}{n}}} + \sum_i \frac{AJ_{01,i}}{N\left[1+\left(\frac{AJ_{01,i}}{B}\right)^n\right]^{\frac{1}{n}}} \quad (5)$$

Table 1
Fitting parameters for various fitting types, cell types, and illumination conditions.

Fitting+cell type, illumination condition	A	B [A/cm^2]	C [A/cm^2]	n
PC1D, BSF-type, AM 1.5	$2*10^{10}$	$2.7*10^{-2}$	$3.87*10^{-2}$	0.42
780 nm	$1.8*10^{9}$	$2.9*10^{-2}$	$3.55*10^{-2}$	0.65
850 nm	$3*10^{9}$	$3.2*10^{-2}$	$3.66*10^{-2}$	0.8
940 nm	$9*10^{9}$	$3.9*10^{-2}$	$4.13*10^{-2}$	0.95
LBIC, BSF-Type, AM 1.5	$1*10^{9}$	$1*10^{-2}$	$3.74*10^{-2}$	1
780 nm	$8*10^{8}$	$7*10^{-3}$	$3.69*10^{-2}$	1
960 nm	$3.9*10^{9}$	$2.4*10^{-2}$	$3.99*10^{-2}$	1
PC1D, PERC, AM 1.5	$2.7*10^{9}$	$2.1*10^{-2}$	$3.5*10^{-2}$	0.7
780 nm	$1.2*10^{9}$	$2.7*10^{-2}$	$3.55*10^{-2}$	0.9
850 nm	$2.5*10^{9}$	$3*10^{-2}$	$3.58*10^{-2}$	0.9
940 nm	$6.5*10^{9}$	$3.4*10^{-2}$	$3.66*10^{-2}$	1
LBIC, PERC, AM 1.5	$1*10^{10}$	$5*10^{-3}$	$4*10^{-2}$	1
780 nm	$5*10^{9}$	$2.4*10^{-3}$	$3.7*10^{-2}$	1
960 nm	$1.5*10^{10}$	$6.3*10^{-3}$	$3.91*10^{-2}$	1

This result contains only the parameters A, B, and n. It will be shown below that, in the most interesting J_{01} range up to several 10^{-11} A/cm^2, parameter n is uncritical and may be chosen as unity. Therefore this improved method also needs only two parameters A and B, whereby parameter B now has a different meaning than in [4].

Note that all these simulation results are made for a homogeneous solar cell. In a real multicrystalline solar cell J_{01} is dominated by recombination-active grain boundaries, see e.g. [12], which have an active spatial extension in the micron range or below. If one image pixel contains such a grain boundary, both J_{01} and J_{sc} are averaged over a region with significantly different values of J_{01}. This averaging would be allowed only if J_{sc} would depend linearly on J_{01}. As Fig. 1 shows, J_{sc} depends linearly on J_{01} only in the low-J_{01} region below $3*10^{-12}$ A/cm^2. However, for higher J_{01}, which holds in the grain boundary positions (see [12]), the dependence becomes strongly sub-linear, namely nearly logarithmic up to 10^{-10} A/cm^2, and then eventually saturates, see Fig. 1(b). Therefore, as has already been discussed in [4], for such an extremely inhomogeneous J_{01} distribution, J_{sc} and J_{01} must be averaged differently in one image pixel. This is the reason why it cannot be expected that the parameters obtained from these homogeneous PC1D simulations also hold for inhomogeneous multicrystalline solar cells. Therefore in the following we will fit LBIC-based J_{sc} data to DLIT-based J_{01} data, which will lead to more realistic fitting parameters for practical applications.

3. Results

LBIC images of a typical multicrystalline BSF-type cell (J_{sc}=34 mA/cm^2) and a p-type multicrystalline PERC cell (J_{sc}=35.5 mA/cm^2) were made at wavelengths of 405, 532, 658, 780, 960, and 980 nm by using a LOANA setup, see [13]. From these monochromatic EQE images, J_{sc} images at AM 1.5 were derived by using the method of Padilla et al. [2]. These two cells were also imaged by DLIT using an InfraTec [14]

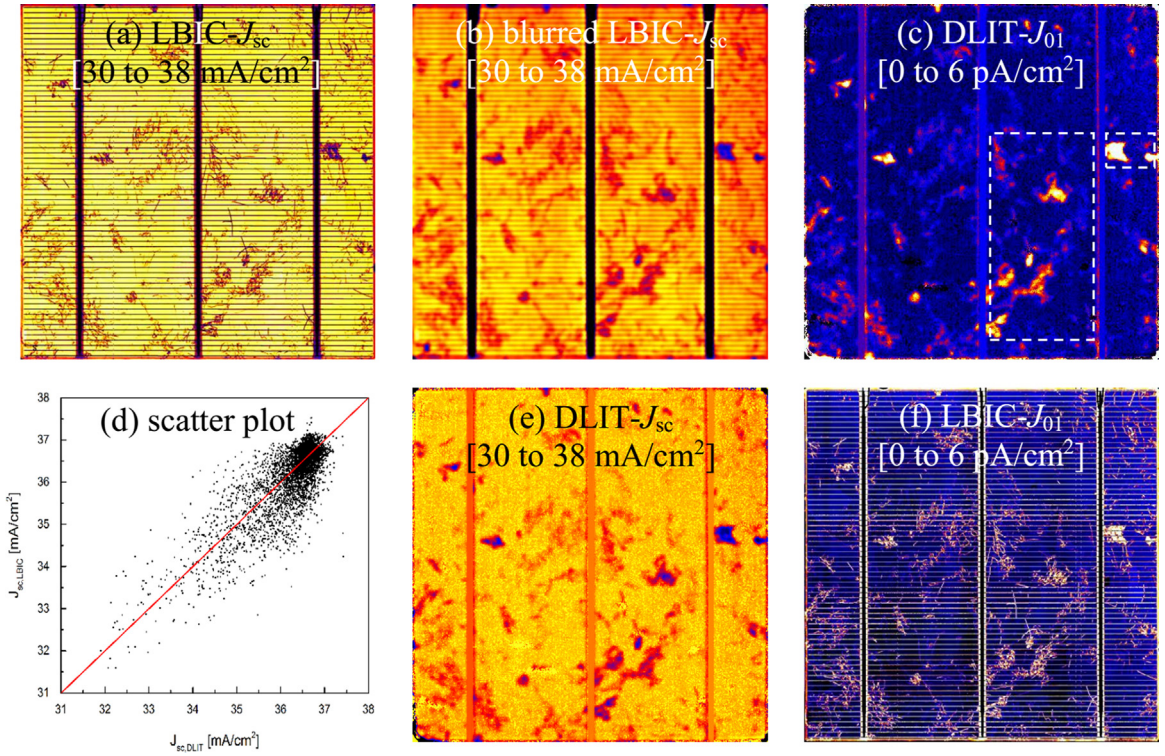

Fig. 2. Fitting results for the BSF-type cell: (a) LBIC-based AM 1.5 J_{sc} image, (b) artificially blurred LBIC-based AM 1.5 J_{sc} image, (c) DLIT-J_{01}, (d) scatter plot, (e) DLIT-simulated J_{sc}, (f) LBIC-simulated J_{01}. All scaling ranges are indicated.

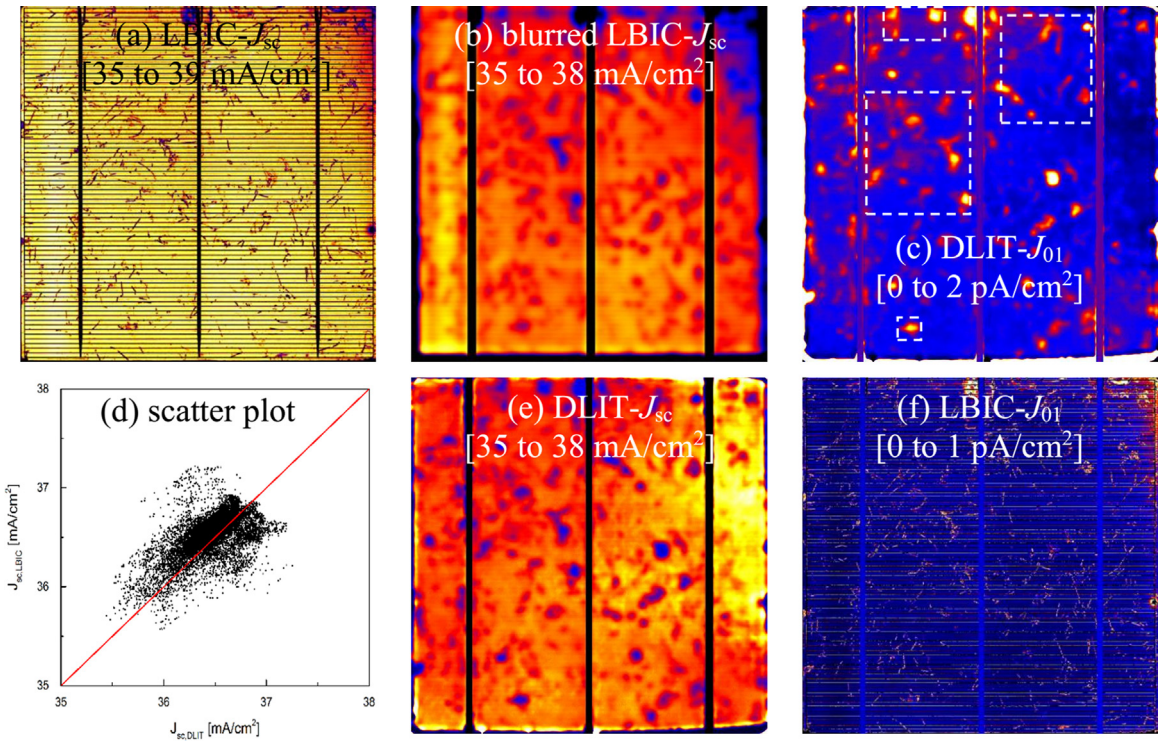

Fig. 3. Fitting results for the PERC-type cell: (a) LBIC-based AM 1.5 J_{sc} image, (b) artificially blurred LBIC-based AM 1.5 J_{sc} image, (c) DLIT-J_{01}, (d) scatter plot, (e) DLIT-simulated J_{sc}, (f) LBIC-simulated J_{01}. All scaling ranges are indicated.

PV-LIT system at its highest possible lock-in frequency of 50 Hz. These DLIT images were evaluated using the "Local I-V 2″ method [5,15] leading to images of J_{01} with a spatial resolution in the order of 1 mm. By applying the scatter plot method described in [4] to Eq. (3), the DLIT-simulated J_{sc} images were fitted to the blurred LBIC-J_{sc} images by using the DLIT-J_{01} images, leading to the fitting parameters also shown in Table 1. The dashed rectangles in Fig. 2(c) mark the regions used for the scatter plot. In these fits, only the image data in the free area between the grid lines and outside of the busbars were used. Therefore, to ensure that the $J_{sc}(J_{01})$ data simulated by (4) match these data, the assumed global J_{sc} has to be increased by a few % to the measured one, as already been mentioned in [4]. For our example we had to increase the global J_{sc} by 3.8%.

In these fittings to experimental data the highest J_{01} values appeared at $1.5*10^{-11}$ A/cm^2. The parameter n did not influence the fitting results measurably up to this J_{01} range, instead the non-linear behavior was only governed by parameter B. Therefore the parameter n was assumed to be unity for all these fittings to LBIC data. Thus, the new method also contains only the two parameters A and B, whereby B now has another meaning than in the old method [4]. Table 1 also contains the monochromatic fitting parameters for 780 nm and 960 nm wavelength. Fig. 2 shows the results of the fitting procedure for AM 1.5 for the BSF-type cell and Fig. 3 for the PERC cell. Here (a) shows the LBIC-based J_{sc} images, (b) the same images artificially blurred to match the DLIT resolution, (c) the DLIT-J_{01} images, (d) the scatter plots, which were used for fitting the parameters A, B, and C, and (e) shows, as the main result of this work, the J_{sc} images simulated from the DLIT-based J_{01} images (c) after Eq. (5) using only the parameters A and B and the slightly increased $<J_{sc}>$.

If we know the dependence of J_{sc} on J_{01}, we may also calculate J_{01} from J_{sc}, hence from an LBIC image. The inverse function of (3), assuming $n=1$, is:

$$J_{01,i} = \frac{BC - BJ_{sc,i}}{AJ_{sc,i} + AB - AC} \tag{6}$$

Figs. 2 and 3(f) show the results of this procedure applied to the AM 1.5 J_{sc} images in (a) by using the LBIC-based fitting parameters in Table 1. We see that, at least in Fig. 2, the agreement with the DLIT-based J_{01} images in (c) is quite good, but the spatial resolution of LBIC-J_{01} is much better than that of DLIT-J_{01}. Of course, in the regions shadowed by the gridlines and busbars, artifacts appear. Note that the fitting parameters A, B, and C in (6) depend on the device type and on the illumination conditions including the intensity. Note also that these parameters were obtained here by averaging over relatively large pixels containing an inhomogeneous J_{01} and J_{sc} distribution. It is possible that these fitting parameters are not optimum anymore for the high resolution case. Astonishingly, the average value of LBIC-J_{01} in the left indicated region of Fig. 2(f) over the regions outside of the gridlines is only 9% higher than the average of DLIT-J_{01} in this region of Fig. 2(c).

The correlations shown in Fig. 3 for the PERC cell are not as good as those in Fig. 2 for the BSF cell. Since the dark currents are generally smaller in the PERC cell than in BSF cells, we have used a lower lock-in frequency for the DLIT measurement (10 instead of 50 Hz) in order to obtain a higher signal. Therefore the thermal blurring is larger in this case, and also the LBIC image in Fig. 3 (b) had to be artificially blurred more strongly. Since in this cell the LBIC contrasts were generally lower, the shadowing action of the gridlines visible in Fig. 3(a) was relatively stronger than in Fig. 2. Therefore the upper scaling limits of (a) and (b) are slightly different here. Though in Fig. 3 the qualitative correlation between the DLIT- and the LBIC-based J_{sc} is also given, the quantitative correlation is not as good as that in Fig. 2. We believe that this is caused by the injection intensity dependence of the lifetime, which is known to be much stronger in PERC than in BSF cells

(see [16]). Note that LBIC is measured under J_{sc} condition, where the excess carrier concentration in the bulk is low, but DLIT is measured close to V_{oc} condition. If different types of defects show different injection dependencies of their recombination activity, they will lead to a different contrast in DLIT-J_{sc} than in LBIC-J_{sc}.

4. Discussion and conclusions

In this contribution a new empirical procedure to convert J_{01} images into J_{sc} images and vice versa is introduced. The parameters of this method are fitted to PC1D simulations and to DLIT-based J_{01} and LBIC-based J_{sc} images of a standard BSF-type and a PERC solar cell. For deriving J_{sc} from J_{01}, if the average value of J_{sc} is known, the method needs only two fitting parameters A and B. If J_{01} is to be derived from a J_{sc} image, three fitting parameters A, B, and C are necessary. All these parameters scale linearly with the illumination intensity and thus with the global value of J_{sc}.

As the scatter plots in Figs. 2 and 3(d) show, the method proposed here shows a distinct scatter and seems to work more accurately for standard than for PERC cells. A general problem of this method, besides the injection intensity dependence of the lifetime mentioned above, is the very different spatial resolution of DLIT and LBIC imaging, which complicates the cross-correlation of these two methods when determining the fitting parameters. Here we have blurred the high-resolution LBIC images to compare them more reliably to the low-resolution DLIT-based J_{01} images. It was already discussed in [4] and again here above that this binning is problematic, since the local effective lifetime (which governs the LBIC signal) and J_{01} actually have to be averaged in a different way. While in low lifetime regions the LBIC signal can only be zero in extreme cases, J_{01} may increase unlimitedly. Another argument for the limited accuracy of this method is that the LBIC signal (in particular the AM 1.5 LBIC signal, which contains contributions from various wavelengths) reacts differently than J_{01} to defects lying in different depths of the cell. The inverse method to calculate J_{01} from LBIC-based J_{sc} is especially prone to artefacts. Whenever a J_{sc} value larger than parameter C appears (since the fitting procedure was performed in another region of the cell), Eq. (6) leads to negative values of J_{01}. Therefore the quantitative accuracy of the method proposed here should not be overestimated.

Nevertheless, the method provides a significant improvement to the assumption of a homogeneously distributed J_{sc}, which is often made in local efficiency analysis (see [6,17]), and also an improvement to the simple quadratic approach used before in [4]. It will be implemented in future versions of the "Local I-V 2″ software for performing DLIT-based local efficiency analysis of solar cells [6,15]. In contrast to a previously proposed PL method for predicting J_{sc} [18], which has recently been shown to be inaccurate since it relied on the model of independent diodes [[7]; note the different scaling ranges of Fig. 2(a) and (c) in [18]], the method proposed here can be expected to be more accurate.

Acknowledgements

The authors are grateful to InfraTec GmbH Dresden [14] for providing and further developing the PV-LIT system used for the DLIT investigation. The authors acknowledge the financial support by the German Federal Ministry for Commerce and Energy and by industry partners within the research cluster "SolarLIFE" (Grant number 325763 D). The content is in the responsibility of the authors.

References

[1] J. Marek, Light beam-induced current characterization of grain boundaries, J. Appl. Phys. 55 (1984) 318–326.
[2] M. Padilla, B. Michl, B. Thaidigsmann, W. Warta, M.C. Schubert, Short-circuit current density mapping for solar cells, Sol. Energy Mater. Sol. Cells 120 (2014) 282–288.
[3] F. Fertig, J. Greulich, S. Rein, Spatially resolved determination of the short-circuit current density of silicon solar cells via lock-in thermography, Appl. Phys. Lett. 104 (2014) 201111.
[4] O. Breitenstein, F. Fertig, J. Bauer, An empirical method for imaging the short circuit current density in silicon solar cells based on dark lock-in thermography, Sol. Energy Mater. Sol. Cells 143 (2015) 406–410.
[5] O. Breitenstein, Nondestructive local analysis of current-voltage characteristics of solar cells by lock-in thermography, Sol. Energy Mater. Sol. Cells 95 (2011) 2933–2936.
[6] O. Breitenstein, Local efficiency analysis of solar cells based on lock-in thermography, Sol. Energy Mater. Sol. Cells 107 (2012) 381–389.
[7] O. Breitenstein, J. Bauer, D. Hinken, K. Bothe, The reliability of thermography- and luminescence-based series resistance and saturation current density imaging, Sol. Energy Mater. Sol. Cells 137 (2015) 50–60.
[8] PC1D, Version 5.9, ⟨http://www.engineering.unsw.edu.au/energy-engineering/pc1d-software-for-modelling-a-solar-cell⟩.
[9] P.A. Basore, Extended spectral analysis of internal quantum efficiency, in: Proceedings of the 23rd IEEE Photovoltaic Specialists Conference, Louisville, 1993, pp. 147–152.
[10] J.H. Werner, S. Kolodinski, U. Rau, J.K. Arch, E. Bauser, Silicon solar cell of 16.8 μm thickness and 14.7% efficiency, Appl. Phys. Lett. 62 (1993) 2998–3000.
[11] O. Breitenstein, The physics of industrial crystalline silicon solar cells, in: Gerhard P. Willeke, Eicke R. Weber (Eds.), Advances in Photovoltaics, Volume 2, Elsevier/AP, Burlington, 2013, pp. 1–75.
[12] S. Rißland, O. Breitenstein, High resolution saturation current density imaging at grain boundaries by lock-in thermography, Sol. Energy Mater. Sol. Cells 104 (2012) 121–124.
[13] ⟨http://www.pv-tools.de/products/loana-system/loana-start.html⟩.
[14] ⟨http://www.infratec-infrared.com/⟩.
[15] ⟨http://www.maxplanckinnovation.de/en/⟩.
[16] D. Chen, W. Deng, J. Dong, F. Ye, H. Zhu, H. Li, Y. Jiang, B. Gao, M. Zhong, Y. Cui, Y. Chen, Y. Yang, Z. Feng, P.P. Altermatt, P.J. Vanderlinden, 21.40% efficient large area screen printed industrial PERC solar cell, in: Proceedings of the 31st EU PVSEC, Hamburg, 2015, pp. 334–340.
[17] C. Shen, H. Kampwerth, M. Green, T. Trupke, J. Carstensen, A. Schütt, Sol. Energy Mater. Sol. Cells 109 (2013) 77–81.
[18] O. Breitenstein, H. Höffler, J. Haunschild, Photoluminescence image evaluation of solar cells based on implied voltage distribution, Sol. Energy Mater. Sol. Cells 128 (2014) 296–299.